

Absolute ionisation cross sections for electrons incident on  $O^+$ ,  $Ne^+$ ,  $Xe^+$  and  $Ar^{i+}$  ( $i=1,\dots,5$ ) ions

This content has been downloaded from IOPscience. Please scroll down to see the full text.

1980 J. Phys. B: At. Mol. Phys. 13 1877

(<http://iopscience.iop.org/0022-3700/13/9/018>)

View [the table of contents for this issue](#), or go to the [journal homepage](#) for more

Download details:

IP Address: 128.3.131.212

This content was downloaded on 06/11/2015 at 20:32

Please note that [terms and conditions apply](#).

## Absolute ionisation cross sections for electrons incident on $O^+$ , $Ne^+$ , $Xe^+$ and $Ar^{i+}$ ( $i = 1, \dots, 5$ ) ions†

A Müller‡, E Salzborn‡, R Frodl§, R Becker§, H Klein§ and H Winter||

‡ Institut für Kernphysik, Universität Giessen, D-6300 Giessen, West Germany

§ Institut für Angewandte Physik, Universität Frankfurt, D-6000 Frankfurt, West Germany

|| Institut für Allgemeine Physik, Technische Universität Wien, A-1040 Wien, Austria

Received 3 August 1979, in final form 5 November 1979

**Abstract.** Absolute ionisation cross sections for electrons incident on  $O^+$ ,  $Ne^+$ ,  $Xe^+$  and  $Ar^{1+}, \dots, Ar^{5+}$  ions have been measured at electron energies  $E_e$  between the ionisation threshold  $E_i$  and 830 eV. The measurements have been performed with crossed electron and ion beams. The comparison of the data for  $O^+$  and  $Ne^+$  with results of Aitken and Harrison and Dolder *et al*, respectively, shows agreement within the combined experimental errors. The measured cross sections for ionisation of  $Ar^{i+}$  ions can be reproduced within  $\pm 20\%$  by the empirical formula

$$\sigma_{i,i+1} = 1.4 \times 10^{-13} \frac{\ln(E_e/E_i)}{E_e E_i} (\text{eV})^2 \text{ cm}^2$$

for the charge states  $i = 1$  up to  $i = 5$ .

### 1. Introduction

Interest in absolute cross sections for the ionisation of atoms and ions arises in the development of ion sources, in controlled nuclear fusion research, and in astrophysics. Since nearly all measurements have so far been limited to atoms or ions of charge one and two (Kieffer and Dunn 1966, Dolder and Peart 1976) there is an important need to extend this work to ions of higher charge (Lorenz 1978).

Two kinds of experiments have been reported up to now for the investigation of electron impact ionisation of multiply (more than doubly) charged ions:

(i) the EBIS work of Donets and co-workers (Donets 1976) and the hollow-beam experiments of Hasted and Awad (1972), Hamdan *et al* (1978) where cross sections are deduced from trapped ion yields and

(ii) crossed-beam measurements for multiply charged carbon, nitrogen and oxygen ions of Crandall *et al* (1977, 1979).

Although there are several semi-empirical formulae to describe electron impact ionisation of atoms and ions (e.g. Drawin 1961, Lotz 1967, Becker *et al* 1972) and although theoretical work has been done for more than six decades now (e.g. Thomson 1912, Bethe 1930, Salop 1976) it is still a problem to predict cross sections at least near the threshold by better than a factor of two (McDowell 1977).

† Work supported by Gesellschaft für Schwerionenforschung (GSI), D-6100 Darmstadt, West Germany.

To provide new experimental data for ionisation processes of multiply charged ions by electron impact we have set up a crossed-beam experiment which has two outstanding features. First, we can produce beams of multiply charged ions with low metastable content and second, a high perveance electron gun has been developed with both a high and well defined electron current density and constant electric potential in the region of electron-ion collisions. With this gun it is possible to obtain high ionisation rates and much better signal to background ratios than in earlier crossed-beam experiments. Moreover, processes with low cross sections, and hence low reaction rates, are made accessible to quantitative investigations. The only shortcoming of this unmodulated crossed-beam experiment is its limited accuracy at low signal to background ratios ( $<0.1$ ).

A detailed presentation of the present experiment will be published elsewhere (report of Gesellschaft für Schwerionenforschung (GSI), Darmstadt).

## 2. Experimental method and apparatus

### 2.1. General

Figure 1 shows a schematic view of the apparatus. A similar arrangement has been described already for the measurement of electron-transfer cross sections in collisions of highly charged ions with atoms and molecules (Klinger *et al* 1975). Neutral gas or vapour is fed into the electron beam ion source (3) (Clausnitzer *et al* 1975) from a vacuum tank (1). Multiply charged ions are continuously extracted and accelerated from the source by a voltage between 5 and 10 kV. Two pairs of electric field plates (4) and an einzel lens (5) are used to steer and focus the ion beam on the entrance aperture (6) of a  $90^\circ$  double focusing magnet (7) which separates the ions into beams of given charge and mass. Behind a collimator (8) ions of a given type then pass perpendicularly

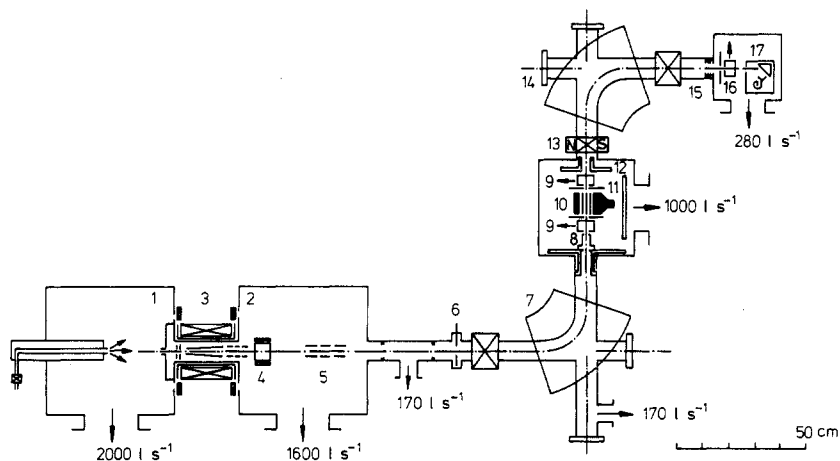


**Figure 1.** Schematic view of the total experimental arrangement: 1, vacuum tank with gas feed system; 2, vacuum tank with deflecting plates (4) and einzel lens (5); 3, electron beam ion source; 6, iris aperture; 7, analysing magnet; 8, ion collimator; 9, movable Faraday cups; 10, electron gun; 11, aperture; 12, liquid- $N_2$  cooled copper plates; 13, steering magnet; 14, analysing magnet; 15, stray particle suppressing electrodes; 16, Faraday cup; 17, single particle detector.

through a flat electron beam (10) of variable energy. Some of the ions are ionised by electron impact and their final charge state is analysed by a second identical magnet (14). Behind this magnet ion currents can be measured alternatively with a Faraday cup (16) or a single particle counting detector (17). A small horizontal magnetic field (13) between the collision region and the second magnet serves for the vertical adjustment of the emerging ion beam to the detector. Four ring electrodes (15) are mounted in front of the Faraday cup (16) and the single particle detector (17) to suppress secondary electrons and stray ions.

The intersection region of the electron and ion beams is sketched in figure 2. The ion beam (about 0.1 cm diameter) is completely embedded in the flat electron beam. Details of geometry and operation of the electron gun are given in § 2.3.

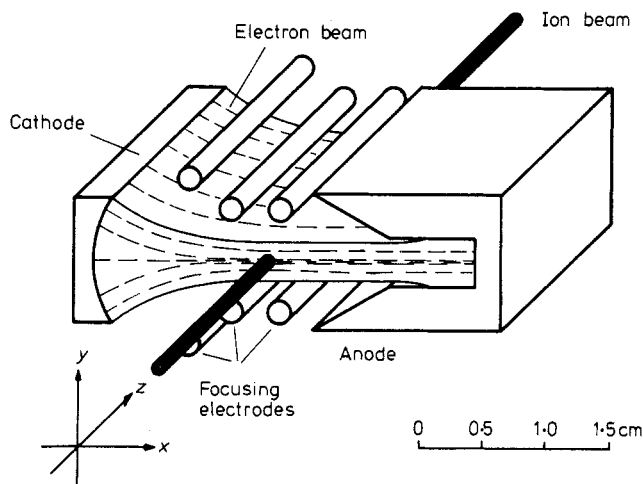


Figure 2. Perspective view of the ion beam crossing the electron gun.

The reaction chamber is pumped by a  $3000 \text{ l s}^{-1}$  freon baffled oil diffusion pump yielding a residual gas pressure of about  $5 \times 10^{-8}$  Torr. The pressure can be reduced to the  $10^{-9}$  Torr range by sublimating titanium on liquid-nitrogen cooled copper plates (12) installed above the pump and at the side walls of the vacuum chamber. During operation of the electron gun the pressure is about  $1 \times 10^{-8}$  Torr and the pressure in the magnet chambers and the remaining beam transport system is  $10^{-7}$  Torr or better.

## 2.2. Ion source and transport

In the electron-beam ion source, neutral gas is ionised by a dense electron beam with keV energies which is axially confined by a strong magnetic field. Multiply charged ions are continuously extracted in the axial direction. For argon ions charge states up to  $\xi = +9$  and for xenon up to  $\xi = +12$  have been observed (Müller and Salzborn 1979). The energy spread of the ions has been measured to be less than  $30\xi$  eV at an energy of  $10\xi$  keV.

Behind the first analysing magnet (25 cm bending radius) the ion beam is collimated by two apertures (0.4 mm diameter, 85 mm apart). Thus a narrow ion beam with maximum angular width  $0.54^\circ$  is obtained for interaction with the crossing electron beam. The resulting magnetic resolution allows for complete separation of the desired

ion species. In the case of  $\text{Ar}^{5+}$ , however, a possible fraction of  $\text{O}^{2+}$  cannot be separated because of equal mass to charge ratio. It could be shown, however, that the fraction of  $\text{O}^{2+}$  is negligible (Klinger *et al* 1975) because of the low residual gas pressure in the ion source (below  $5 \times 10^{-8}$  Torr).

To achieve optimum transmission of the ion beam through the collimator, two pairs of electric field plates and an einzel lens are installed behind the ion source. For the lower charge states, however, the ion currents provided by the source are too high for proper operation of the single particle detector. It is therefore necessary to reduce the parent beam current by defocusing it in the plane of the collimator. For the cross section measurements incident ion currents of order 1 nA are typical.

Just behind the electron gun ((10) in figure 1) different apertures (11) of 0.05 cm up to 0.4 cm diameter can be set to the beam axis to check the transmission of the ion beam through the interaction region. This measurement is facilitated by two movable Faraday cups (9) in front of and behind the collision region. Moreover, the second analysing magnet has an acceptance angle of at least  $3^\circ$ . By comparing the ion currents measured before and behind this magnet 100% ion transmission could be proved.

### 2.3. Electron gun

In view of the signal to background ratios in the crossed-beam experiments an electron gun is desirable which provides high electron current density and a long interaction path for the ions. A constant potential in the interaction region of the two beams is also demanded for a well defined electron impact energy and to avoid defocusing of the ions.

With these requirements in mind an electron gun was developed (Becker *et al* 1977) by using modified versions of the computer codes of Kirstein and Hornsby (1963) and Herrmannsfeldt (1973). These programs solve Poisson's equation for arbitrary electrode systems with an emitting surface. The modifications take into account the thermal spread of representing trajectories as well as—even in the case of non-uniform emission current density distribution—the proper positioning of the potential minimum which can be regarded as a virtual cathode. Further details will be described elsewhere (Sinz 1979). The result of this calculation is represented in figure 3 which shows a section through the electron gun assembly perpendicular to the crossing ion beam together with electron trajectories and equipotentials.

The electrons are emitted from a cylindrical cathode made of impregnated tungsten with a radius of curvature of 0.8 cm and a length of 6 cm along the ion-beam direction. Pierce angle electrode design at all edges of the emitting surface together with six tungsten rods at proper electric potentials mounted in parallel to the cathode and the ion beam provide an electron beam of  $9.5 \mu\text{A V}^{-3/2}$  perveance. This means a maximum power of 300 W deposited on the water-cooled copper anode at a voltage of 1000 V.

Since the complete electron gun is insulated from ground potential it is possible to shift the potential of the interaction region to any desired value without changing the electron beam properties.

The contour of equipotentials near the ion beam shows that the potential is nearly uniform in this region. This homogeneity results from the interpenetration effects of the differently biased tungsten rods in combination with the potential depression by the electron space charge. In fact, the calculations yield a potential of  $0.83 U_{CA}$  constant to 0.5% over the cross section of the ion beam, where  $U_{CA}$  is the voltage between cathode and anode.

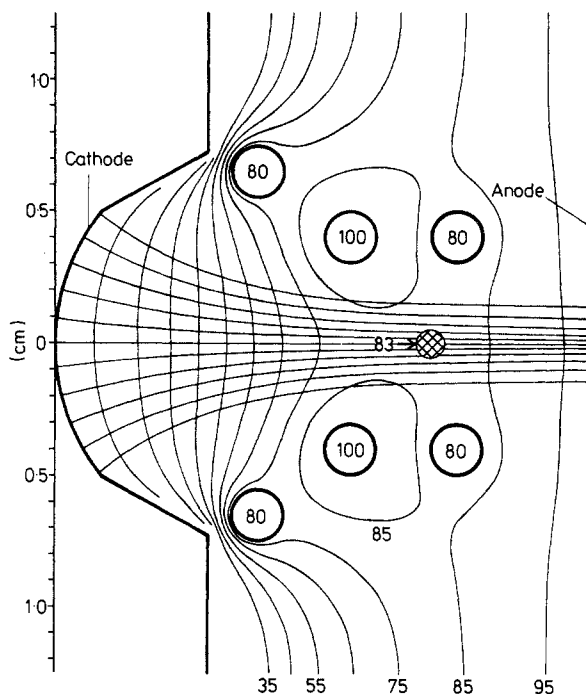


**Figure 3.** Electron trajectories and equipotential lines calculated in a plane perpendicular to the ion beam. The region of ion penetration is cross hatched. The electric potentials applied to the different electrodes are given in percent of the voltage  $U_{CA}$  between cathode and anode.

This potential could also be measured. At different electron energies the potential of the interaction region was kept constant by appropriately biasing the whole gun. The bias was correct when the product ions passed through the analyser magnet in which the field was held constant. These measurements, performed with different ion species, resulted in an experimentally defined electron energy of  $(0.81 \pm 0.03)U_{CA}$  which agrees with the calculated value.

One of the most important parameters in the present experiment is the electron current density distribution in the interaction region. Besides calculations the density distribution has been measured by using a movable scanner (Frodl 1979).

In the midplane of the interaction region a tantalum plate with a narrow slit ( $\approx 0.005$  cm width, 7 cm length) was installed perpendicular to the electron flow. The slit was parallel to the  $x/z$  plane. The scanner was kept at a potential of  $0.83U_{CA}$  with respect to the cathode to minimise its influence on the electron trajectories. Electrons penetrating through the slit were collected by a plate 0.4 cm apart. To suppress secondary electrons a biased plate with a slit of 0.5 cm width was installed in front of the collector plate. By moving the slit in the  $y$  direction the current density distribution was recorded.

As shown from the calculations, by proper electrode design no significant current density variation is to be expected in the  $x$  and  $z$  directions. This is discussed further in § 3. All measured profiles have been integrated and compared with the current emitted by the cathode. The anode current may not be useful for the normalisation, because of secondary electron emission from the collector. By the comparison of integrated

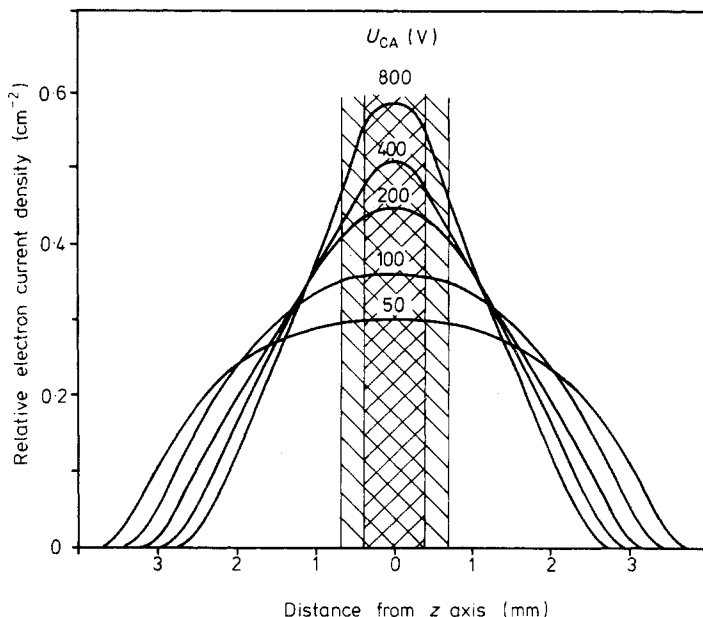


**Figure 4.** Relative current density profiles in the  $y$  direction perpendicular to the ion and electron beam for different anode voltages. The cross hatched regions show the ion beam widths just at the entrance and exit of the electron beam.

current density distributions and the electron current emitted by the cathode an effective slit width of  $58 \pm 3 \mu\text{m}$  was determined which compares well with microscopic inspection.

The current density profiles normalised to the cathode current are shown in figure 4 for voltages  $U_{CA}$  of 50, 100, 200, 400 and 800 V. They are very much affected by the transverse motion of electrons emitted with initial thermal velocities from the cathode. The boundaries of the ion beam, as defined by the collimator, are indicated by cross-hatched regions. From the measured profiles the current density decrease at the maximum ion beam radius of 0.07 cm was found to amount to 97.5, 96, 91, 81 and 79% for voltages of 50, 100, 200, 400 and 800 V, respectively. For electron energies above 200 eV the variation of the electron current density within the ion beam may exceed 10%, therefore this variation must be considered in the determination of the cross sections (for details see § 3). The measured peak current density normalised to the cathode current is in agreement with the calculated value for all energies to better than 5%, as may be seen from figure 5.

#### 2.4. Ion detector

Because of the low rates of product ions in the crossed-beam experiments a single particle counting technique has been chosen instead of electric current measurements.

The detector used (see figure 6) consists of a metal plate (1) which serves as a converter of fast particles to secondary electrons and a channel electron multiplier (2) (Valvo B419 BL-01). The detector is shielded from stray particles and photons by a grounded metal box and the converter plate (1) is kept at a potential of about  $-3.5 \text{ kV}$  to reject slow electrons from the ion-beam line. Secondary electrons released by

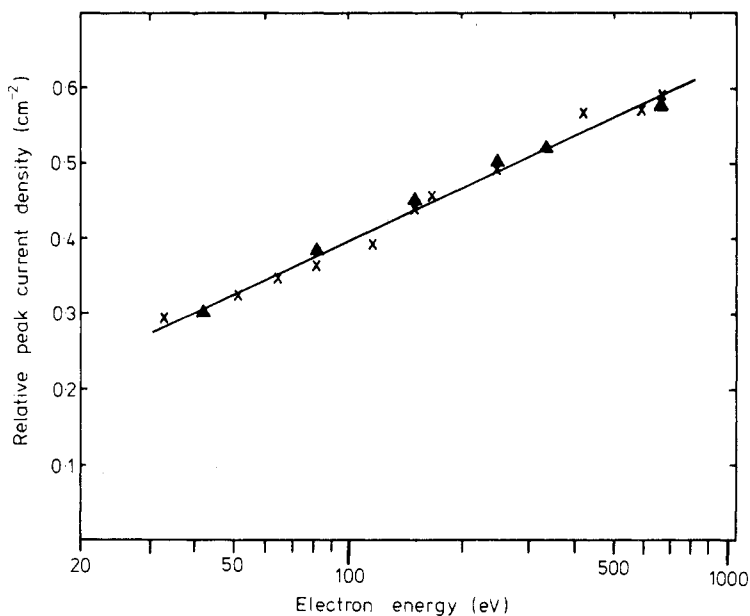


**Figure 5.** Measured (×) and calculated (▲) peak current density normalised to the cathode current for different electron energies.

energetic ions are accelerated and focused by a potential difference of +500 V between plate (1) and the channeltron entrance. At the exit of the channeltron, which is grounded via the input resistor of the preamplifier, charge pulses of about  $10^8$  electrons are obtained. The dark rate of the detector is about 1 count per second.

For a quantitative measurement of particle fluxes the counting efficiency of the detector had to be determined. This calibration has been performed in two ways. In the more general method particle fluxes were reduced in a defined way by using small

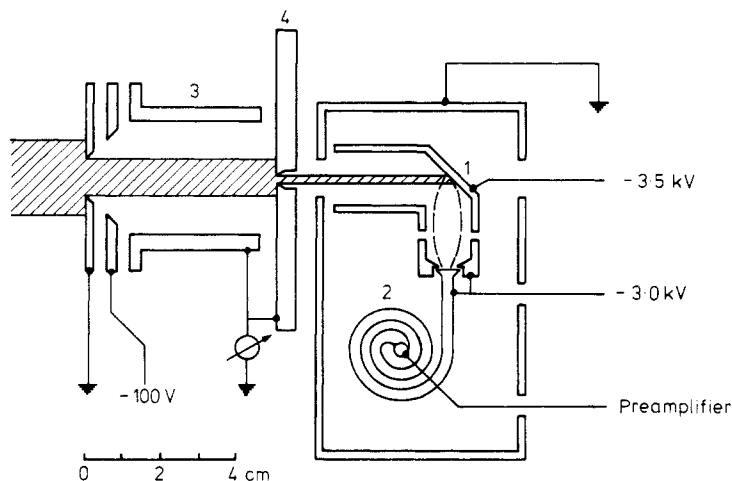


**Figure 6.** The single particle detector and the calibration arrangement: 1, converter plate; 2, channel electron multiplier; 3, Faraday cup with movable bottom plate 4 and a small hole ( $30\mu\text{m}$  diameter) for ion beam scanning and probing of the movable detector.

apertures. The current of an ion beam (some 10 pA) with defined diameter (1 cm) is measured with a Keithley electrometer and a Faraday cup (3) which has a small hole (30  $\mu\text{m}$  in diameter) in the movable bottom plate (4). The small ion fluxes ( $<10^4 \text{ s}^{-1}$ ) passing through this hole can be measured with the single particle detector.

The incident ion beam does not have a uniform current density and therefore its distribution is measured by moving the bottom plate of the cup together with the detector over the whole cross section of the incident beam. By comparison of the integrated measured particle fluxes with the ion current collected in the Faraday cup the efficiency of the detector then was determined (Fricke 1978, Eichenauer 1979). These measurements resulted in counting efficiencies of about 95% for ions of keV energies.

The overall efficiency of the detector is then easily determined by moving only the detector behind the hole in a plane perpendicular to the now fixed narrow ion beam. This procedure is equivalent to scanning the detector with an ion probe. The counting rates measured with a constant ion flux on the detector exhibit an effective detecting area of about 1 cm diameter with uniform efficiency of 95%. This area is large enough to guarantee a complete collection of product ions in the present crossed-beam experiment.

A second way to measure the counting efficiency of the single particle detector was provided by the crossed-beam experiment itself: for the ionisation of  $\text{Xe}^{1+}$  ions the product ion rates are sufficiently high to be measured with a Faraday cup ( $0.2\text{--}0.8 \times 10^{-12} \text{ A}$ ). Thus an absolute measurement of cross sections is possible with the technique described in the next section. By reducing the parent  $\text{Xe}^{1+}$  beam current—which is still measured by a Faraday cup—the flux of the ionised ions becomes sufficiently low to be measured by the single particle detector ( $<10^4 \text{ s}^{-1}$ ). The results of these two cross section measurements are shown in figure 7. Assuming a 93% efficiency for the single particle detector, both measurements are in accordance with each other. This efficiency value compares well with the value obtained with the more general method.

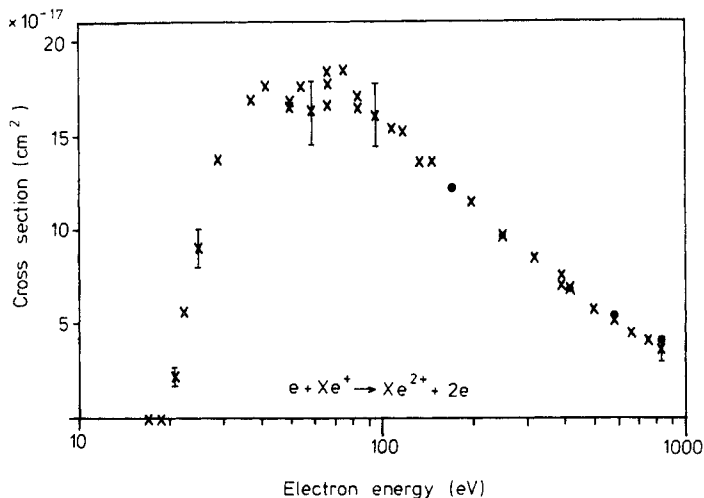


**Figure 7.** Cross sections for the ionisation of  $\text{Xe}^{1+}$  ions measured with the single particle detector (x) in comparison with the measurement by a Faraday cup (●).

### 3. Determination of cross sections from measured data

By definition the reaction rate  $R$  of a collision process between ions and electrons with densities  $n_i$  and  $n_e$  and relative velocity  $v_{i,e}$  depends on the corresponding cross section  $\sigma(v_{i,e})$ :

$$R = \int n_i n_e v_{i,e} \sigma(v_{i,e}) dV. \quad (1)$$

In the electron gun electrons with velocities of  $4 \times 10^8$  to  $1.7 \times 10^9$  cm s<sup>-1</sup> collide with ions of  $8.6 \times 10^6$  (5 keV Xe<sup>1+</sup>) to  $5 \times 10^7$  (50 keV Ar<sup>5+</sup>) cm s<sup>-1</sup>, therefore the electron velocity  $v_e$  differs from the collision velocity  $v_{i,e}$  by less than 1%, and hence  $v_{i,e}$  can be replaced by  $v_e$  in equation (1). Furthermore,  $v_e$  is constant to better than  $\pm 0.25\%$  within the collision volume by virtue of the potential homogeneity of the gun. The laminar flow of electrons in this region makes  $n_e$  independent of  $x$ , the electron flow direction. In the ion-beam direction  $z$  the observation of the electron collector pattern revealed an electron beam extension of  $5.96 \pm 0.05$  cm with sharp boundaries, which corresponds within 0.7% to the cathode length. Therefore, the electron density can also be assumed to be independent of  $z$ . Even if the electron density had depended on  $z$ , the measurements of the current density profiles, as reported in § 2.3 would have integrated it leading to correct reaction rates. In evaluating equation (1) we conclude that  $n_e$  varies only according to the current density distribution in dependence on  $y$ , the direction perpendicular to both ion and electron beams.

The scanning of the ion beam behind the electron gun by different apertures shows that for diameters of 1 mm or less the transmitted ion current is proportional to the square of the diameter. This gives confidence that the ion beam has uniform density, because of the very small apertures of the collimator being used during the experiment. By the collimator action ions may be found in the electron beam in a truncated cone with an entrance diameter of  $2r_1 = 0.08$  cm, exit diameter  $2r_2 = 0.14$  cm and length  $l = 6$  cm. At a position  $z$  the radius of the cone is  $r_z = r_1 + (r_2 - r_1)z/l$  and the area of this circle is uniformly filled with ions of density  $n_i = I_i / (e \zeta_0 v_i \pi r_z^2)$ , where  $I_i$ ,  $\zeta_0$  and  $v_i$  denote the ion current, its initial charge state and its velocity, respectively.

Taking everything together equation (1) becomes:

$$R = \frac{I_i \sigma(v_e)}{e^2 \zeta_0 \pi v_i} \int_0^l \frac{1}{r_z^2} dz \int_{-r_z}^{+r_z} dx \int_{-\sqrt{(r_z^2 - x^2)}}^{+\sqrt{(r_z^2 - x^2)}} j_e(y) dy. \quad (2)$$

The current density measurements, as reported in § 2.3, showed that the dependence  $j_e(y)$  within the interaction volume is well represented by a parabola of peak current density  $j_0$  and width parameter  $r_0$ . Additionally, to study the effect of misalignment a shift  $y_0$  of the current density parabola versus the ion beam is introduced

$$j_e(y) = j_0 \{1 - [(y - y_0)/r_0]^2\}. \quad (3)$$

This enables integration of (2) yielding

$$R = \frac{I_i \sigma(v_e) l j_0}{\zeta_0 e^2 v_i} \left( 1 - \frac{y_0^2}{r_0^2} - \frac{r_1^2 + r_1 r_2 + r_2^2}{12 r_0^2} \right). \quad (4)$$

Obviously, the bracket contains the reduction of the peak current density by misalignment and by averaging  $j_e$  over the ion flow cone.

The width parameter  $r_0$  varies considerably with energy and amounts for the worst case (highest energy) to  $r_0 = 0.15$  cm. Misalignment was manifested by lack of transmission and the necessary corrections never exceeded  $y_0 = 0.05$  cm. With these values equation (4) gives a maximum reduction of the counting rate by misalignment of 11% and by calculating the average value of  $j_e$  of 3%. This is taken into account as an additional error contribution being largest for high electron energies. Unfortunately, the present experimental conditions do not allow for a direct measurement of the electron and ion beam overlap integral. By taking  $R$  as the measured reaction rate in counts  $s^{-1}$ ,  $I_i$  as the initial ion current in A,  $\zeta_0$  as the initial charge state of this current,  $l$  as the length of the ion path in the electron beam in cm,  $v_i$  as the ion velocity in  $cm s^{-1}$ ,  $j_0/I_e$  as the peak electron current density normalised to the cathode current in  $cm^{-2}$  (see figure 5),  $I_e$  as the measured cathode current in A, and  $e = 1.602 \times 10^{-19}$  As, we determine cross sections from

$$\sigma(v_e) = \frac{e^2 \zeta_0 v_i R}{I_i I_e (j_0/I_e)}. \quad (5)$$

#### 4. Discussion of measuring procedure and experimental uncertainties

(i) The condition of single collisions is fulfilled if the product of ionisation cross sections  $\sigma$ , of electron flux density  $j_e/e$ , and the time of flight  $\tau$  of the ions through the electron beam is small compared to unity. With  $\sigma < 10^{-16} cm^2$ ,  $j_e/e < 9 \times 10^{17} cm^{-2} s^{-1}$  and  $\tau < 7 \times 10^{-7} s$  in this experiment we have  $\sigma\tau(j_e/e) < 7 \times 10^{-5} \ll 1$ . A more detailed analysis of charge-state distributions of ions passing through an electron beam shows that for  $\tau(j_e/e) < 10^{14} cm^{-2}$  the condition for single collisions is already fulfilled safely (cf Müller *et al* 1976a). This is of special importance for the investigation of multiple ionisation processes.

(ii) Defined chemical composition and charge purity of the parent ion beam are guaranteed by the high resolution of the analysing system. This has been verified by additional investigations described by Klinger *et al* (1975).

The present experiment aimed to measure cross sections for the ionisation of ground state ions but the parent beam may contain ions in long-lived excited states. The flight time of ions between ion source and interaction volume ranges between about 5  $\mu s$  for 50 keV  $Ar^{5+}$  ions and 25  $\mu s$  for 5 keV  $Xe^+$  ions and this does not permit the decay of metastable ions.

A qualitative test for the presence of metastables in the parent beam has been performed by using both electron capture and electron stripping collisions in two successive gas cells as described by Gilbody (1978). None of these experiments (Müller *et al* 1976b) gave any hint for metastable ions being extracted from the electron-beam ion source. On the other hand, the methods were sensitive enough to give evidence for the population of metastable states of  $Ne^+$  ions in charge-transfer collisions (Seim 1978). This is remarkable since until recently (Noerdlinger and Dynan 1975) the existence of metastable states in  $Ne^+$  ions has been questioned (see e.g. Dolder *et al* 1963).

The absence of metastable ions in the beam may be due to the exceptionally low gas pressure ( $< 10^{-5}$  Torr) and high electron impact energy (3 keV) in the source. Hence, in the ion source almost no ion-atom collisions can occur which would produce ions in metastable states and, moreover, Bethe theory predicts (Bethe 1930) that the probability for forbidden transitions falls off more rapidly with electron energy than for

allowed transitions. This is supported by the recent investigations of Varga and Winter (1978), Winter and Varga (1979). Long-lived highly excited states may survive the flight time from the source to the interaction region but ions with high principal quantum numbers would be quenched by accelerating fields.

A second check for the presence of metastable ions in the parent ion beam is provided by the crossed-beam experiment itself: at electron energies below the ionisation threshold no significant counting rates (significant with respect to counting statistics and other experimental uncertainties—see also § 5) are measured, as can be seen for instance in figure 7. If there were, for example, a fraction of 5% metastable ( $5d\ ^4D_{7/2}$ ,  $^4F_{7/2}$  or  $^4F_{9/2}$ ; excitation energy  $\approx 12$  eV)  $\text{Xe}^{1+}$  ions in the beam, according to the Gryzinski theory (1965) an apparent cross section of about  $5 \times 10^{-18}$  cm<sup>2</sup> at 15 eV electron energy should be observed. The experiment, however, exhibits a strong increase of the ionisation cross section only above the ionisation threshold of 21.2 eV for ground state  $\text{Xe}^{1+}$  ions showing that a possible fraction of metastable ions in the parent beam is well below 5%. The situation for other projectiles is similar.

(iii) The ion and electron currents are measured with Keithley electrometers. An uncertainty of  $\pm 2\%$  of full scale reading from the electrometers is quoted by the manufacturer.

The ion velocity is determined by the first analysing system with an estimated possible error of less than  $\pm 1\%$ .

The design of the electron gun is such that there is a uniform potential to  $\pm 0.5\%$  in the interaction region and hence, the electron impact energy is well defined.

(iv) For the measurement of a cross section  $\sigma$  it is necessary to provide complete transmission of both parent and product ions to the detector. By using a narrow parent ion beam ( $\approx 0.1$  cm diameter) and a detector with an effective area of 1 cm diameter together with the properties of the electron gun and the acceptance angle of the analysing magnet of at least  $3^\circ$  one can be sure to fulfil the condition of complete transmission.

This can be checked experimentally by using different apertures for the ion beams behind the interaction volume: it has been observed that the parent ion beam is nearly completely transmitted already through a rear aperture of 0.1 cm diameter, whereas the product ion flux increases with increasing diameter of the aperture up to 0.3 cm and then remains constant. With the fact of complete transmission through the analysing system this proves as well complete transmission of the product ions through the electron beam for a rear aperture of more than 0.3 cm diameter. During the actual measurements an aperture of 0.4 cm diameter has been used.

The observation of flat topped current peaks behind the second analysing system additionally guarantees the complete collection of the ions in the detector (see figure 8).

(v) Incident ions are ionised by collisions with background gas as well as with electrons. A further background may arise from photons produced by impact of ions and electrons on the walls.

To reduce the background problems the residual gas pressure in the interaction volume was generally kept below  $2 \times 10^{-8}$  Torr during the measurements. The background is determined by switching off the electron beam. This method, however, can only be used if the electron beam does not cause additional background, e.g. by desorbing gas from the anode and by producing photons or soft x-rays which might reach the detector.

The influence of electromagnetic radiation excited by the electron beam can be checked during the experiment since the background should not be affected by the

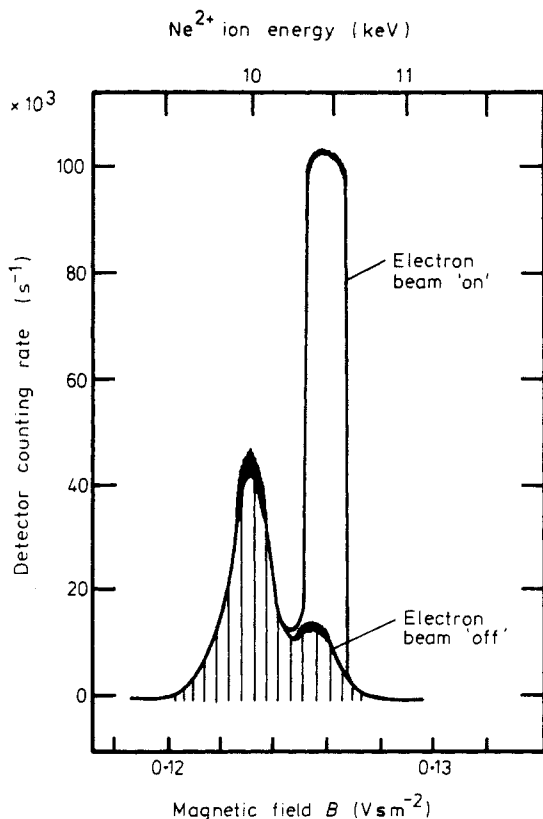


**Figure 8.** Spectrum of magnetically analysed  $\text{Ne}^{2+}$  ions measured with crossed beams of 10 keV  $\text{Ne}^+$  ions (16.3 nA) and 243 eV electrons (53 mA). The observed counting rates for electron beam 'off' are indicated by vertical hatching lines.

magnetic field of the product ion analyser. Since the detector background at magnetic fields, where no ions are transmitted, is not changed when the electron beam is switched on and off, one can be sure to have no problems with electron beam excited radiation (see also figure 8).

In order to investigate the possible influence of ion stripping collisions in the residual gas, we have measured cross sections for the electron stripping of different ion species in various target gases. As an example figure 9 shows the stripping of  $\text{Ne}^+$  ions in  $\text{O}_2$  which is a most effective stripper gas (Seim 1978). The data were taken with the experimental set-up described by Klinger *et al* (1975) and they are shown together with the high energy measurements of Brackmann *et al* (1970), (see Dehmel *et al* 1973). In the energy range of about 10 keV which is of interest for the present experiment, the stripping cross section  $\sigma_{1,2}^{\text{str}}$  depends strongly on the projectile energy.

With these data and the measured cross section  $\sigma_{1,2}$  for the ionisation of  $\text{Ne}^+$  by electron impact (Dolder *et al* 1963) an estimate of the expected signal to background ratios in the present experiment can be made. The background counting rate  $U$  from ion stripping collisions is given by

$$U = \frac{I_i}{e} \sigma_{1,2}^{\text{str}} \mu = \frac{I_i}{e} \sigma_{1,2}^{\text{str}} p l_{\text{eff}} / (kT) \quad (6)$$

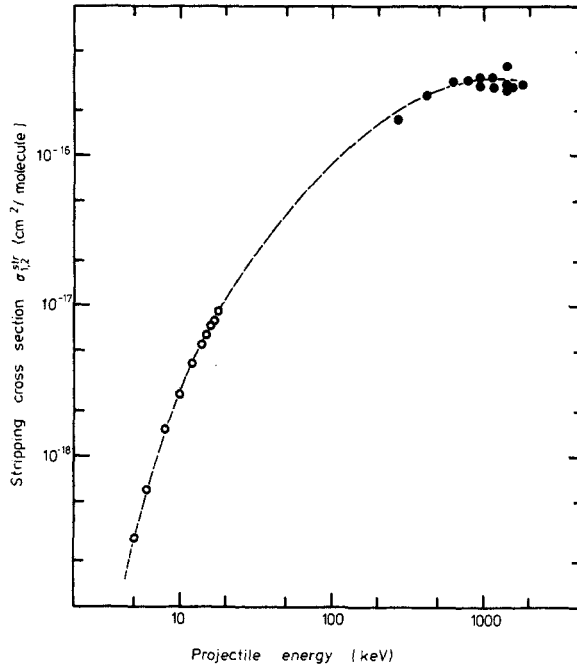


**Figure 9.** Stripping cross sections for  $\text{Ne}^+$  ions in  $\text{O}_2$ . The low energy data ( $\circ$ ) are measured at the present facility where the electron gun was replaced by a gas cell (Seim 1978) and the high energy data ( $\bullet$ ) were measured by Brackman *et al* (1970, see Dehmel 1973).

where  $I_i$  is the parent  $\text{Ne}^+$  ion current,  $\sigma_{1,2}^{\text{str}}$  the stripping cross section of  $\text{Ne}^+$  ions,  $\mu$  the target thickness seen by the incident ions in the collision chamber,  $p$  the gas pressure in the collision chamber,  $l_{\text{eff}}$  the effective length of the collision chamber,  $k$  is Boltzmann's constant and  $T$  is the absolute temperature of the collision gas.

With equation (5) one obtains

$$r = \frac{R}{U} = \frac{\sigma_{1,2} j_0 I_i / v_i}{e \sigma_{1,2}^{\text{str}} I_i p l_{\text{eff}} / (kT)}. \quad (7)$$

As seen by figure 5 the peak electron current density  $j_0$  can be fairly well expressed as a function of  $U_{\text{CA}}^{3/2}$  and one gets

$$r \approx 2.8 \times 10^{13} \text{ V}^{-3/2} \text{ cm}^{-2} \text{ s}^{-1} \sigma_{1,2} U_{\text{CA}}^{3/2} \frac{l k T}{v_i \sigma_{1,2}^{\text{str}} p l_{\text{eff}}}.$$

For an estimate of the influence of the constant residual gas pressure the ratio  $r$  is calculated as a function of the electron energy  $E_e$  for an assumed maximum target thickness in the collision chamber of  $2 \times 10^{-8}$  Torr 50 cm/( $kT$ ) and an energy of 10 keV for the  $\text{Ne}^+$  ions:

$$r \approx 9 \times 10^{13} \sigma_{1,2} E_e^{3/2} (\text{eV})^{-3/2} \text{ cm}^{-2}. \quad (8)$$

Because of the shape of the cross section function  $\sigma_{1,2}(E_e)$  the ratio  $r$  is smallest near the ionisation threshold ( $r \approx 0.1$  for  $E_e = 50$  eV), it increases to  $r \approx 8$  for  $E_e = 200$  eV and further up to  $r \approx 39$  for  $E_e = 800$  eV electron energy. The conclusion is that the

separation of the constant background considered here should be no experimental problem if the counting statistics are sufficient.

A more difficult problem is the desorption of gas from the anode of the electron gun. Because of the power deposited by the electron beam outgassing of the electron collector may be expected. In separate experiments this problem has been investigated (Stummer 1978, Frodl 1979). The pressure variation by the electron gun has been measured with an ionisation gauge screened from stray electrons by electric and magnetic fields. When the electron beam is switched on, the gas pressure rapidly increases depending on the time of undisturbed adsorption. But after a few seconds the adsorbed layers on the water-cooled collector are almost completely removed and after about 30 seconds the pressure has dropped again to a constant value. There remains, however, a pressure increase which was found to be proportional to the electron current—not to the power deposited on the collector. Investigations with a residual gas analyser showed that the increase is due to enhanced fractions of  $H_2$  and CO in the vacuum chamber.

The observed effect may be attributed to the production of secondary electrons and soft x-rays at the collector which can lead to desorption from the surrounding tank walls. The secondary electrons produced can be retained if the anode is kept at a positive potential as was the case in our measurement.

It is obvious from equation (5) and the observed proportionality of the electron beam induced pressure increase with the electron beam current (Stummer 1978) that in the present cross section measurement the relative error arising from this effect is largest for smallest reaction rates, i.e. near the ionisation threshold. Therefore, it is a good check for such errors to take data below the ionisation threshold where an effect of ionised ions apart from metastable parent ions can only arise from additional background caused by the electron beam. In the experiments described in this paper the apparent cross sections below the ionisation threshold were not larger than the fluctuations to be expected from counting statistics and normalisation to the parent beam current.

A further test for the accurate determination of ionisation rates is provided by the following refinement. Since all electrodes of the electron gun are insulated from each other and from ground potential it is possible to shift the potential of the interaction region to any desired value without changing the electron beam parameters. Thus the intersection volume of the colliding beams can be kept, for example, at a positive potential, which decelerates and accelerates the transient ions resulting in a net energy gain or loss, according to the change of charge state within this potential barrier, i.e. inside the electron beam. By using this method it is possible to separate ions stripped outside the electron beam from ions stripped or ionised inside the electron beam.

A spectrum of product  $Ne^{2+}$  ions obtained in this way is shown in figure 8. The pertinent experimental parameters were: residual gas pressure  $p = 2 \times 10^{-7}$  Torr, energy of ions  $E_{ion} = 10$  keV, electron energy  $E_e = 243$  eV, ion current  $I_i = 100$  pA, electron current  $I_e = 57$  mA. The potential of the interaction volume was +443 V. These data have been taken at relatively high residual gas pressure in order to visualise the effects of stripping.

The spectrum shows the ion fluxes of  $Ne^{2+}$  ions arising from incident 10 keV  $Ne^+$  ions with electron beam switched on and off. Two peaks may be observed: one at an analysing field belonging to 10 keV and one at 10.44 keV. The first belongs to ions stripped outside the electron beam, the second to those generated inside the electron

beam. When the electron beam is switched off the first peak remains constant while the second one is reduced to the small fraction of ions stripped inside the interaction zone.

By this method a further reduction of the effective constant background is achieved in the present experiment. Additionally, some further conclusions may be drawn from figure 8. Firstly, the fact that the main stripping peak is not influenced in general by the electron beam proves that the effect of additional outgassing with running electron beam is small indeed. The region of constant potential in the electron gun takes about 25% of the ion path in the vacuum tank. Under stationary conditions the pressure in the electron beam and in the surrounding tank are identical due to the open construction of the electron gun. If there were an additional stripping contribution due to the electron beam the background of the ionisation rates would also change according to those 25%. Because no change in the counting rate resulting from stripping outside of the electron beam was found, no correction had to be made. Secondly, the background beside the ion peak remains constant, which proves that, within the present accuracy, no radiation produced by the electrons affects the detector. Thirdly, the main stripping peak is smeared out showing that stripping collisions are combined with considerable angular deflection of the ions. This fact may additionally reduce this background by incomplete transmission of the stripped ions. On the other hand, the peak of ions produced by electron impact has steep flanks and is flat topped, which clearly proves that this beam is narrow assuring its complete collection by the detector.

For every single cross section measurement the product ion beam has been analysed magnetically to assure—by the method described above—a correct subtraction of background and a complete collection of product ions. In addition, three further tests have been performed to prove the correct measurement of the flux of ions produced by electron impact.

Firstly, the cross sections have been measured with different residual gas pressure between  $1 \times 10^{-8}$  Torr and  $2 \times 10^{-7}$  Torr, thus changing the stripping background. Within the experimental uncertainties no differences could be observed for the measured cross sections.

Secondly, the accelerating voltage for the incident ions was varied between 5 and 10 kV. As can be read e.g. from figure 9, the stripping cross sections change in this range nearly by a factor 10 and thus the stripping background including the effect of additional outgassing is reduced to one tenth for 5 keV  $\text{Ne}^+$  ions compared with 10 keV  $\text{Ne}^+$  ions. Since we could not observe a difference between cross sections measured with ions of different energies, obviously the background is correctly taken into account.

Thirdly, we have checked that the measured cross sections are independent of the incident flux of parent ions as long as the product ion fluxes are below about  $10^4$  counts per second. Above this limit the counting efficiency of the single particle detector begins to decrease.

Unfortunately, it has not yet been possible to measure the parent ion beam and the ionisation product flux simultaneously. By a small drift of the parent ion current during the counting of the product ions errors may arise especially near the ionisation threshold, where the ratio of signal to background is low. For this reason periods of about one minute were used to switch the second magnet between parent and product beam. For low signal to background ratios the two signals were measured alternatively over 10 s. Measuring  $N_T$  counts of product ions in  $t_T$  seconds if the electron beam is switched on and  $N_B$  counts in  $t_B$  seconds if it is switched off the relative error within a

95% confidence limit is given by

$$\frac{\Delta R}{R} = 2 \frac{\sqrt{(N_T/t_T^2) + (N_B/t_B^2)}}{(N_T/t_T) - (N_B/t_B)}. \quad (9)$$

The statistical error in counting is different for every measured cross section because the reaction rate  $N_T/t_T$  is proportional to the cross section and the background  $N_B/t_B$  depends on the charge state and species of the incident ion beam. For example, for the process  $\text{Ar}^{1+} \rightarrow \text{Ar}^{2+}$  at an electron energy of 95.5 eV  $N_T = 3.11 \times 10^5$  counts in  $t_T = 60$  s and  $N_B = 1.2 \times 10^4$  counts in  $t_B = 40$  s were obtained which results in a counting statistic error of less than  $\pm 1\%$ .

At an electron energy of 25 eV  $N_T = 4.13 \times 10^4$  in  $t_T = 30$  s and  $N_B = 3.8 \times 10^4$  in  $t_B = 30$  s were measured which yields an error of  $\pm 16\%$ .

For energies higher than those belonging to respective maximum cross sections the statistical error is lower than 2% for  $\text{Ar}^{1+} \rightarrow \text{Ar}^{2+}$  and  $\text{Ar}^{2+} \rightarrow \text{Ar}^{3+}$ , lower than 3% for  $\text{Ar}^{3+} \rightarrow \text{Ar}^{4+}$  and  $\text{Ar}^{4+} \rightarrow \text{Ar}^{5+}$  and lower than 9% for  $\text{Ar}^{5+} \rightarrow \text{Ar}^{6+}$ . Near the threshold energy the total error is mostly affected by the counting statistic error. At high energies where the electron current density distribution is less uniform the main error arises from a possible misalignment of the electron gun with respect to the ion beam or an inhomogeneity in ion and electron density. The cross sections are underestimated because of both error sources. A reduced transmission of the parent ion beam then indicated misalignment. The necessary corrections never exceeded 0.05 cm. Therefore the error contribution by misalignment is calculated from equation (4) using this value, shown by crosses in its energy dependence in figure 10. The underestimation of

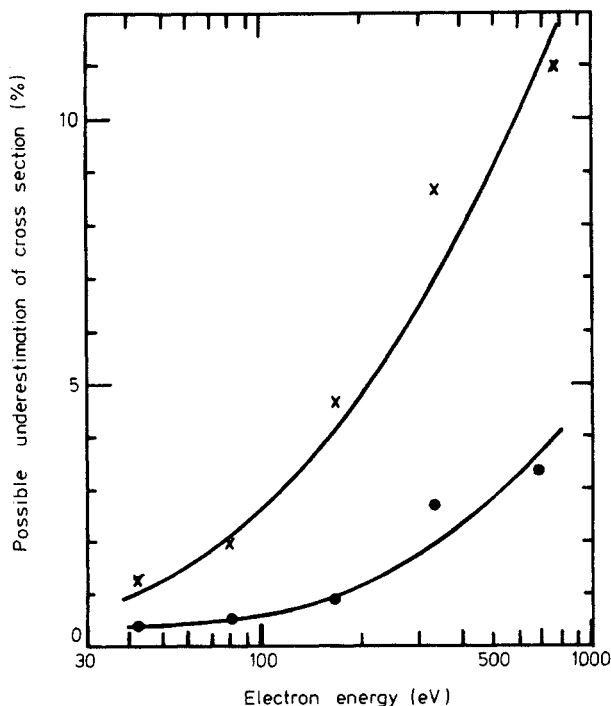


**Figure 10.** Possible underestimation of ionisation cross sections due to misalignment (x) of the gun with respect to the ion beam and due to evaluation of cross sections with peak electron current density (●), respectively, versus the electron energy.

the cross sections by using equation (5) instead of (4) amounts to about 32% of the misalignment error and is also shown in figure 10 by dots.

**Table 1.** Experimental uncertainties.

$n$		$\epsilon_n$ (%)
<i>(a) Cross section</i>		
1	Counting efficiency	$\pm 5$
2	Measurement of parent ion flux	$\pm 2$
3	Stability of ion current (the influence on $\sigma$ depends on the signal to background ratio)	$\pm 4$
4	Measurement of electron current	$\pm 2$
5	Determination of current density	$\pm 6$
6, 7	Misalignment and averaging by non-uniform current density	see figure 10
8	Error from counting statistics above maximum cross section	$< \pm 9$
<i>(b) Electron energy</i>		
	Measurement of the potential	$\pm 2$
	Determination of absolute electron energy	$\pm 3$

The other sources of error  $\epsilon_n$  are listed in table 1. The total error  $\epsilon$  is determined from  $\epsilon = (\sum_{n=1}^8 \epsilon_n^2)^{1/2}$ . For the above example of 25 eV electrons incident on  $Ar^{1+}$  this means  $\epsilon = (0.05^2 + 0.02^2 + 0.04^2 + 0.02^2 + 0.06^2 + 0.005^2 + 0.002^2 + 0.16^2)^{1/2} = 0.19$  according to table 1 and figure 10. At representative electron energies the total error is indicated by bars in the figures of the measured data and also listed in table 2.

### 5. Results

The obtained cross section data are compiled in table 2. Figure 11 shows a comparison of the present results for the ionisation of  $Ne^+$  ions with data of Dolder *et al* (1963). For

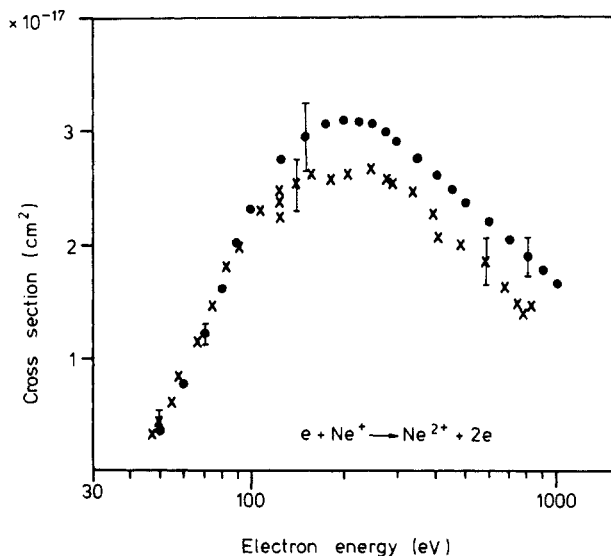


**Figure 11.** Comparison of measured ionisation cross sections for  $Ne^+$  ions (x) with data from Dolder *et al* (1963) (●).

both experiments typical error bars are indicated. Within the combined errors the measurements are in agreement, however, at higher energies both sets of data seem to diverge.

For further comparison with known data cross sections for the ionisation of  $O^+$  ions have been measured at various electron impact energies. The results are shown in figure 12 together with data from Aitken and Harrison (1971). The present cross sections are about 20% below the results of these authors which is again consistent within the errors of both measurements.

The aim of the present investigation was to measure cross sections for the electron impact ionisation of multiply charged ions. Data have been obtained for the following series of processes:  $Ar^{i+} + e \rightarrow Ar^{(i+1)+} + 2e$  with  $i = 1, 2, \dots, 5$ , where the electron

**Table 2.** Electron impact ionisation cross sections.

	Electron energy (eV)	Cross section ( $10^{-17} \text{ cm}^2$ )	Total error (%)	Electron energy (eV)	Cross section ( $10^{-17} \text{ cm}^2$ )	Total error (%)
Xe <sup>1+</sup> to Xe <sup>2+</sup>	20.8	2.2	±19	133	13.6	
	22.4	5.6		145	13.7	
	24.9	9.1	±10	166	12.7	
	29.0	13.8		199	11.6	
	37.3	16.9		249	9.9	
	41.5	17.6			9.9	
	49.8	16.6		315	8.7	
		16.8		390	7.7	
	53.9	17.6			7.3	
	58.1	16.3	±9	415	7.1	+12 -9
	66.4	16.6			7.0	
		18.4		498	5.9	
		17.8		581	5.3	
	74.7	18.4			5.3	
	83.0	16.5		664	4.70	
		17.0			4.67	
	95.4	16.2		747	4.25	
108	15.4	+10 -9	830	4.31	+15 -9	
116	15.3			3.80		
Ne <sup>1+</sup> to Ne <sup>2+</sup>	47.3	0.312		158	2.62	
	49.8	0.423	±19	183	2.58	
	54.8	0.61		207	2.62	
	58.1	0.82	±12	249	2.66	
		0.81		278	2.57	
	66.4	1.14		290	2.54	
	74.7	1.46		340	2.46	
	83.0	1.80		398	2.26	
		1.80		415	2.05	
	91.3	1.99		490	1.99	
	108	2.29		589	1.83	+14 -9
	124	2.46	±11	685	1.61	
		2.23		747	1.47	
	2.36		780	1.41		
141	2.54		830	1.46	+15 -9	
O <sup>1+</sup> to O <sup>2+</sup>	83.0	3.19	±9	166	3.65	
	124	3.55		357	2.75	+12 -9

Table 2.—continued.

	Electron energy (eV)	Cross section ( $10^{-17} \text{ cm}^2$ )	Total error (%)	Electron energy (eV)	Cross section ( $10^{-17} \text{ cm}^2$ )	Total error (%)
Ar <sup>1+</sup> to Ar <sup>2+</sup>	24.9	0.68	±22	83.0	9.0	
		0.64	±31	95.4	8.3	
	26.6	0.472		108	8.1	
	27.4	2.10		124	7.9	
	29.0	2.15		149	7.3	
	29.9	2.44		166	6.9	
		2.80		207	6.1	+10 -9
	31.5	4.28			6.6	
		4.49		249	5.3	
	33.2	5.5			6.1	
	35.7	6.2	±9	290	5.3	
	41.5	8.1		332	4.94	
	49.8	8.8		415	4.15	+13 -9
	58.1	8.9		498	3.55	
	66.4	9.4		664	2.63	+14 -9
74.7	9.5	±10				
	8.7					
Ar <sup>2+</sup> to Ar <sup>3+</sup>	37.3	0.198	±107	74.7	4.49	
	38.2	0.319		91.3	4.32	
	39.0	0.95	±20	108	4.19	±10
	40.7	1.34		124	3.90	
	41.5	1.07		133	3.98	
		1.52		149	3.82	
	42.3	1.10			3.72	
		1.37		166	4.02	
	43.2	1.53			3.53	
		1.65		207	3.70	
		1.30			3.21	
	44.0	2.25		249	3.40	
	45.6	2.44			3.29	
		2.20		266	2.83	
	46.5	2.51		332	2.59	+10 -9
49.8	3.47	±10		2.66		
	3.30		415	2.23		
	3.05		498	1.93		
	2.76		581	1.75		
58.1	3.84		622	1.63		
	3.89		747	1.31	+14 -9	
Ar <sup>3+</sup> to Ar <sup>4+</sup>	56.4	0.123	±24	249	1.63	
	58.1	0.275			1.47	
	60.6	0.56			1.40	
	66.4	0.86	±16		1.46	
	83.0	1.36		290	1.49	
	99.6	1.53		332	1.42	
	124	1.59		373	1.28	+12 -9
	166	1.57	±10		1.24	
		1.64		415	1.15	
		1.59		456	1.11	
		1.64		539	0.96	
		1.69		622	0.87	
	207	1.54		705	0.81	+14 -9

Table 2.—continued.

	Electron energy (eV)	Cross section ( $10^{-17} \text{ cm}^2$ )	Total error (%)	Electron energy (eV)	Cross section ( $10^{-17} \text{ cm}^2$ )	Total error (%)
Ar <sup>4+</sup> to Ar <sup>5+</sup>	74.7	0.191	±15	332	0.71	
	78.8	0.328			0.81	
	83.0	0.471			0.86	
	89.6	0.59		415	0.75	
	99.6	0.74		498	0.61	
	116	0.99	±10	664	0.55	+14 -9
		0.88			0.56	
	149	0.86		780	0.487	
	166	0.91		830	0.456	+15 -9
	199	0.91	±10			
249	0.85					
	0.88					
Ar <sup>5+</sup> to Ar <sup>6+</sup>	124	0.346	±18	332	0.72	
		0.321		349	0.59	+13 -11
	133	0.442		415	0.57	
	145	0.57			0.62	
	166	0.71	±24		0.55	
		0.52		498	0.59	
		0.55		581	0.52	
	207	0.66			0.50	
		0.61		664	0.417	
	249	0.71	±14	830	0.408	+15 -10
290	0.58					

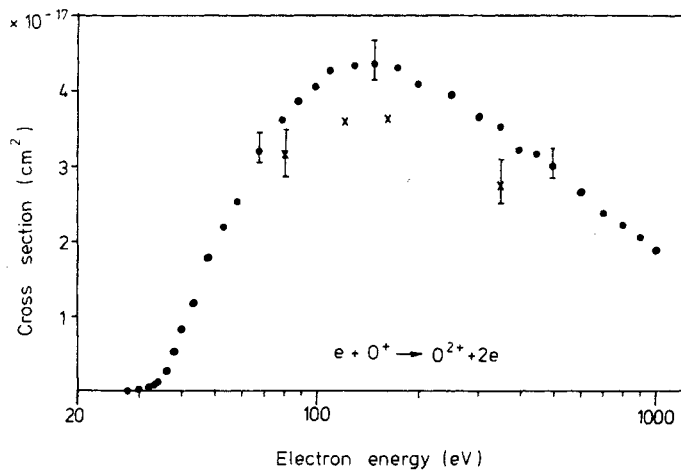


Figure 12. Comparison of measured ionisation cross sections for O<sup>+</sup> ions (×) with data obtained by Aitken and Harrison (1971) (●).

energies  $E_e$  ranged from the respective ionisation threshold  $E_i$  up to  $E_e = 830$  eV. The measured cross sections are shown in figure 13.

The shape of the observed data suggests the application of a simple empirical formula to represent the cross sections:

$$\sigma_{i,i+1} = \frac{A}{(E_e E_i)} \ln(E_e/E_i). \quad (10)$$

It turns out that for all investigated charge states the present measurements can be reproduced with one common fit parameter  $A = 1.4 \times 10^{-13} \text{ cm}^2 (\text{eV})^2$ . Cross sections calculated from equation (10) are shown by full curves in figure 13.

The plot of  $\sigma_{i,i+1} E_e$  as a function of  $\ln E_e$  yields the experimental ionisation potentials  $E_i$  as the intersections of the fit lines with the energy axis.

For the calculation of cross sections these fitted values of  $E_i$  are used and shown in table 3 together with data of Moore (1970).

The deviations of measured and calculated cross sections are within a limit of 20%. This is rather surprising, since the same  $A$  has been taken for all data. By the

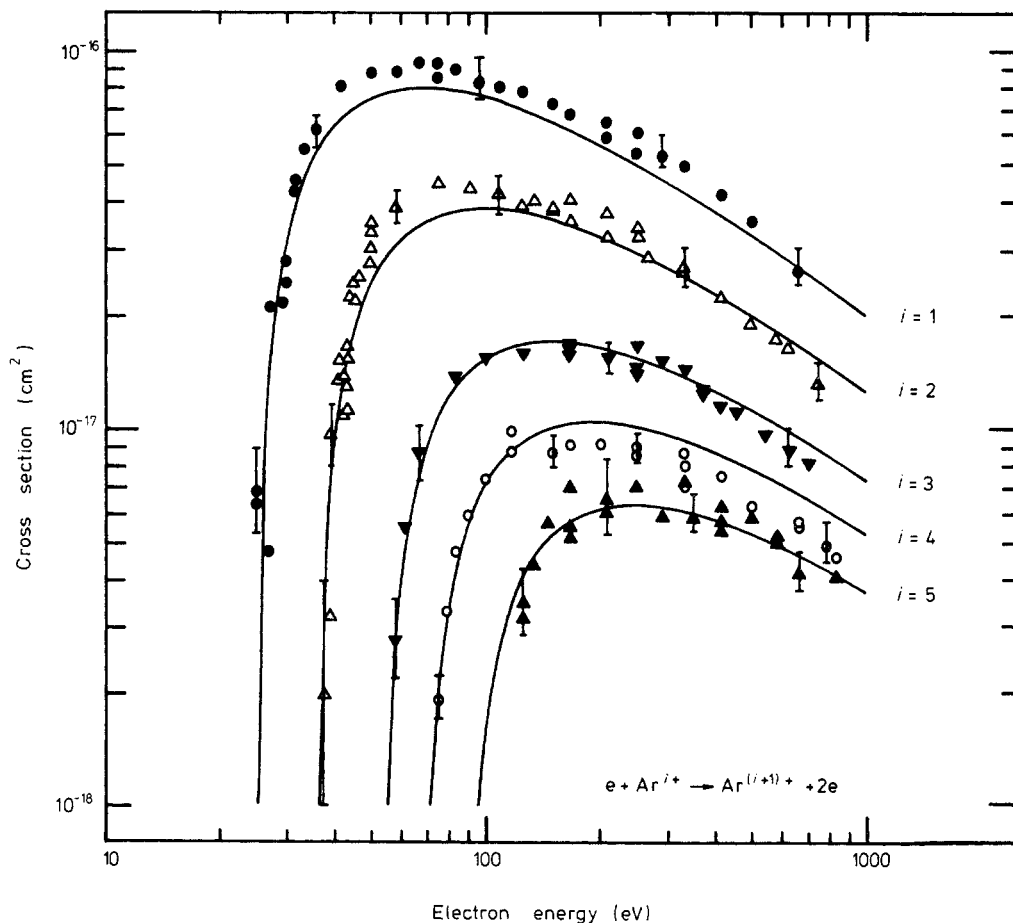


**Figure 13.** Cross sections for the ionisation processes  $\text{Ar}^{i+} + e \rightarrow \text{Ar}^{(i+1)+} + 2e$  with  $i = 1, 2, \dots, 5$ . The full curves are calculated from formula (10).

**Table 3.** Observed threshold energies (eV) and known ionisation potentials from spectroscopic data.

Process	Experimental data this work	Moore (1970)
Ar <sup>1+</sup> → Ar <sup>2+</sup>	25 ± 1	27·6
2 <sup>+</sup> → 3 <sup>+</sup>	36 ± 1	40·7
3 <sup>+</sup> → 4 <sup>+</sup>	54 ± 2	59·8
4 <sup>+</sup> → 5 <sup>+</sup>	69 ± 2	75·0
5 <sup>+</sup> → 6 <sup>+</sup>	89 ± 3	91·0

approximation given we intend to give a simple formula which represents the measured data with acceptable errors (see also Becker *et al* 1972). Such formulae are especially convenient for the calculation of the charge state balance in plasmas (cf Müller *et al* 1976a).

Figure 13 may indicate an increase of the cross section  $\sigma_{1,2}$  at electron energies above 200 eV. Unfortunately, the present accuracy of the measurements does not allow us to decide whether this is a significant effect. There are theoretical predictions by Salop (1976) and by Hahn (1977) and experimental evidence has been given both by Peart and Dolder (1975) and by Crandall *et al* (1979) that the ionisation of ions may be influenced by the excitation of autoionising states resulting in structured cross section curves. On the other hand, previous experiments for the ionisation of Ar<sup>+</sup> (Woodruff *et al* 1978, Hasted and Awad 1972) do not show this relative increase at 200 eV. Measurements with improved accuracy should clarify the situation.

Comparison of the present cross sections  $\sigma_{1,2}$  for Ar<sup>+</sup> with the results of Woodruff *et al* (1978) again gives a 20% deviation.

Donets (1976) has measured the cross sections  $\sigma_{4,5} = 3 \cdot 1 \times 10^{-18} \text{ cm}^2$  and  $\sigma_{5,6} = 2 \cdot 05 \times 10^{-18} \text{ cm}^2$  for Ar<sup>4+</sup> and Ar<sup>5+</sup>, respectively, at an electron energy  $E_e = 2 \cdot 5 \text{ keV}$ . An extrapolation of the present results according to equation (10) yields  $\sigma_{4,5} = 2 \cdot 9 \times 10^{-18} \text{ cm}^2$  and  $\sigma_{5,6} = 2 \cdot 05 \times 10^{-18} \text{ cm}^2$ .

A comparison of the present data with cross sections calculated on the basis of the binary encounter approximation by Salop (1976) for Ar<sup>*i*+</sup> ions ( $i \geq 3$ ) shows agreement within 20% for Ar<sup>5+</sup>, whereas the cross sections for Ar<sup>4+</sup> ions are overestimated up to 80% by the theory.

### Acknowledgment

The authors are indebted to Professor K T Dolder for helpful discussions and his efforts to improve this manuscript.

### References

- Aitken K L and Harrison M F A 1971 *J. Phys. B: Atom. Molec. Phys.* **4** 1176–88  
 Becker R, Frodl R and Klein H 1977 *Workshop on EBIS and Related Topics, Darmstadt* (Darmstadt: Wolf and Klein) GSI-P-33-77 pp 75–6  
 Becker R, Klein H and Schmidt W 1972 *IEEE Trans. Nucl. Sci.* **NS-19** 125–30  
 Bethe H 1930 *Ann. Phys., Lpz.* **5** 325–400

- Clausnitzer G, Klinger H, Müller A and Salzborn E 1975 *Nucl. Instrum. Meth.* **128** 1–7
- Crandall D H, Phaneuf R A, Hasselquist B E and Gregory D C 1979 *J. Phys. B: Atom. Molec. Phys.* **12** L249–56
- Crandall D H, Phaneuf R A and Taylor P O 1978 *Phys. Rev. A* **18** 1911–24
- Crandall D H, Taylor P O and Phaneuf R A 1977 *Proc. 10th Int. Conf. on the Physics of Electronic and Atomic Collisions* (Paris: Commissariat à l'Énergie Atomique) pp 1086–7
- Dehmel R C, Chan H K and Fleischmann H H 1973 *Atom. Data* **5** 231–89
- Dolder K T, Harrison M F A and Thonemann P C 1963 *Proc. R. Soc. A* **274** 546–51
- Dolder K T and Peart B 1976 *Rep. Prog. Phys.* **39** 693–749
- Donets E D 1976 *Int. Conf. on Heavy Ion Sources, Gatlinburg, IEEE Trans. Nucl. Sci.* **NS-23** 897–903
- Drawin H-W 1961 *Z. Phys.* **164** 513–21
- Eichenauer H 1979 *Staatsexamensarbeit* University of Giessen
- Fricke J 1978 *Diploma Thesis* University of Giessen
- Frodl R 1979 *Thesis* University of Frankfurt
- Gilbody H B 1978 *Low-energy Ion Beams, Salford 1977: Inst. Phys. Conf. Ser.* **38** 156–68
- Gryzinski M 1965 *Phys. Rev.* **138** A336–58
- Hahn Y 1977 *Phys. Rev. Lett.* **39** 82–4
- Hamdan M, Birkinshaw K and Hasted J B 1978 *J. Phys. B: Atom. Molec. Phys.* **11** 331–7
- Hasted J B and Awad G L 1972 *J. Phys. B: Atom. Molec. Phys.* **5** 1719–34
- Herrmannsfeldt W B 1973 *Stanford Linear Accelerator Centre, SLAC* 166 Electron trajectory program
- Kieffer L J and Dunn G H 1966 *Rev. Mod. Phys.* **38** 1–35
- Kirstein P T and Hornsby J S 1963 *A FORTRAN Programme for the Numerical Analysis of Curvilinear Electrode Systems with an Emitting Surface* (Geneva: CERN European Organization for Nuclear Research) CERN 63-16
- Klinger H, Müller A and Salzborn E 1975 *J. Phys. B: Atom. Molec. Phys.* **8** 230–8
- Lorenz A (organiser) 1978 *Invited papers at IAEA advisory meeting, Vienna 1976: Phys. Rep.* **37C** No 2
- Lotz W 1967 *Z. Phys.* **206** 205–11
- McDowell M R C 1977 *Comm. Atom. Molec. Phys.* **7** 23–33
- Moore C E 1970 NSRDS-NBS 34 (Washington DC: US National Bureau of Standards)
- Müller A, Klinger H and Salzborn E 1976a *Nucl. Instrum. Meth.* **140** 181–8
- 1976b *J. Phys. B: Atom. Molec. Phys.* **9** 291–3
- Müller A and Salzborn E 1978 *Low-energy Ion Beams, Salford 1977: Inst. Phys. Conf. Ser.* **38** 169–74
- 1979 *Nucl. Instrum. Meth.* **164** 607–8
- Noerdlinger P D and Dynan S E 1975 *Astrophys. J. Suppl.* **283** 185
- Peart B and Dolder K T 1975 *J. Phys. B: Atom. Molec. Phys.* **8** 56–62
- Salop A 1976 *Phys. Rev. A* **14** 2095–102
- Seim W 1978 *Diploma Thesis* University of Giessen
- Sinz W 1979 *Diploma Thesis* University of Frankfurt, in preparation
- Stummer K 1978 *Diploma Thesis* University of Frankfurt
- Thomson J J 1912 *Phil. Mag. Suppl.* **6** **23** 449–57
- Varga P and Winter H 1978 *Phys. Rev. A* **18** 2453–8
- Winter H and Varga P 1979 *Proc. 11th Int. Conf. on the Physics of Electronic and Atomic Collisions* (Kyoto: Society for Atomic Collision Research) pp 204–5
- Woodruff P R, Hublet M-C and Harrison M F A 1978 *J. Phys. B: Atom. Molec. Phys.* **11** L305–8